JOURNAL OF BACTERIOLOGY, Jan. 2006, p. 370–377 Vol. 188, No. 2
0021-9193/06/$08.00+0 doi:10.1128/JB.188.2.370–377.2006

Nanoscale Characterization and Determination of Adhesion Forces of *Pseudomonas aeruginosa* Pili by Using Atomic Force Microscopy

Ahmed Touhami,[1] Manfred H. Jericho,[1]* Jessica M. Boyd,[2] and Terry J. Beveridge[3]

Department of Physics and Atmospheric Science, Dalhousie University, Halifax, Nova Scotia, Canada B3H 3J5[1]; National Research Council of Canada Institute for Marine Biosciences, 1411 Oxford St., Halifax, Nova Scotia, Canada B3H 3Z1[2]; and Canadian Bacterial Disease Network, National Centre of Excellence, Department of Microbiology, College of Biological Science, University of Guelph, Guelph, Ontario, Canada N1G 2W1[3]

Received 25 August 2005/Accepted 31 October 2005

Type IV pili play an important role in bacterial adhesion, motility, and biofilm formation. Here we present high-resolution atomic force microscopy (AFM) images of type IV pili from *Pseudomonas aeruginosa* bacteria. An individual pilus ranges in length from 0.5 to 7 μm and has a diameter from 4 to 6 nm, although often, pili bundles in which the individual filaments differed in both length and diameter were seen. By attaching bacteria to AFM tips, it was possible to fasten the bacteria to mica surfaces by pili tethers. Force spectra of tethered pili gave rupture forces of 95 pN. The slopes of force curves close to the rupture force were nearly linear but showed little variation with pilus length. Furthermore, force curves could not be fitted with wormlike-chain polymer stretch models when using realistic persistence lengths for pili. The observation that the slopes near rupture did not depend on the pili length suggests that they do not represent elastic properties of the pili. It is possible that this region of the force curves is determined by an elastic element that is part of the bacterial wall, although further experiments are needed to confirm this.

Pili, also known as fimbriae, are thin, hairlike appendages on the surface of many microorganisms, especially gram-negative and gram-positive bacteria. They perform a variety of different functions, for example, aiding genetic transfer via conjugation (e.g., F pili of *Escherichia coli*), movement across surfaces via twitching (e.g., the type IV pili of *Pseudomonas aeruginosa*), and adherence to a variety of surfaces (e.g., type IV pili of *P. aeruginosa*). These surfaces for adherence can consist of inanimate materials (e.g., ceramics, glasses, and minerals, etc.) or biomaterials (e.g., epithelial surfaces, red blood cells, yeasts, and fungi) (1, 3, 14, 21, 31). Pili play an essential role in bacterial colonization (and are colonization factors), since they are used in the initial stages of biofilm formation, in which reversible adherent forces are important (6, 9, 13, 19, 28, 33).

Adhesive type IV pili are thin filaments expressed by diverse gram-negative bacteria, such as *P. aeruginosa*, pathogenic *Neisseria* spp., enteropathogenic *E. coli*, *Vibrio cholerae*, and *Moraxella bovis*. This group of pili has been extensively studied because they are implicated in a variety of functions, including biofilm formation, bacteriophage adsorption, and adhesion to host cell surfaces (3, 4, 28). Moreover, some type IV pili represent good model systems since their genetics, secretion, and complicated assembly are reasonably well known. Some adhesive pili are structurally quite complicated because they are assembled sequentially out of a number of different secreted proteins. An extreme example is the P pilus of uropathogenic *E. coli*, which adheres to the Gal-α-(1-4)-Gal receptor of human epithelial kidney cells, and its PapC, PapH, PapA, PapK, PapE, PapF, and PapG (adhesin) proteins (27).

* Corresponding author. Mailing address: Department of Physics and Atmospheric Science, Dalhousie University, Halifax, Nova Scotia, Canada B3H 3J5. Phone: (902) 494-2316. Fax: (902) 494-5191. E-mail: jericho@fizz.dal.ca.

For a number of years, we have been interested in *P. aeruginosa* biofilms and have been studying the adhesion forces during biofilm formation by atomic force microscopy (AFM) (30, 35). It was important to both visualize the pili of our *P. aeruginosa* PAO1 strain and determine the adhesive forces of piliated cells to an inanimate surface (e.g., mica). These type IV pili are semiflexible rodlike fibers formed by the ordered association of thousands of identical pilin subunits plus several accessory proteins, all arranged in a helical manner (3, 4). This helical filament is about 5 to 6 nm in diameter and up to several micrometers in length. The flexibility and strength of a pilus is primarily determined by the bonding forces between pilin subunits as determined by the helicity of the assembly. Since these *P. aeruginosa* type IV pili are also involved in twitching motility (34), these intersubunit bonds are presumably readily broken to accommodate reversible depolymerization and assembly of the filament. Recently, Skerker et al. (29) showed that type IV pili in *P. aeruginosa* can be extended or retracted at rates of about 0.5 μm s^{-1} and also flexed by Brownian motion, exhibiting a persistence length of about 5 μm.

Rapid progress in applying AFM to biological systems has been made in the past few years, indicating that the instrument is taking root in the microbiological science community (5, 15, 32). Although AFM was initially developed as an imaging tool, it has rapidly evolved into a quantitative probe for the measurement of interaction forces between biomolecules and for determining their physical properties. In particular, AFM probes, functionalized with microbial cells, have been used to characterize a variety of bacterial surface interactions (7, 16, 26). In this report, we show that AFM is an exquisitely sensitive tool (i) for examining the general morphology and structure of the pili fibers at high resolution and (ii) for understanding the physical nature of pili by determining the interaction forces between these filaments and hard mica surfaces as well as the

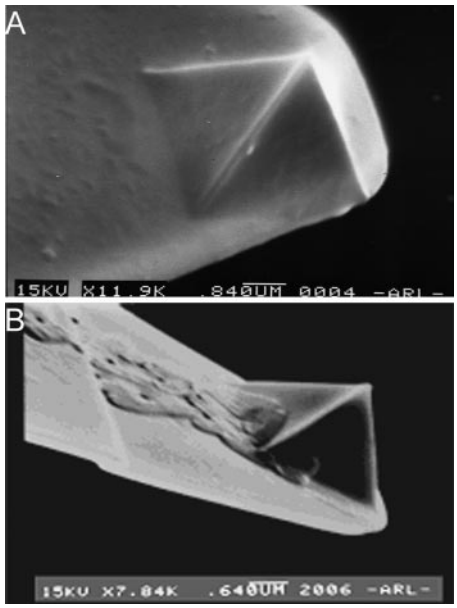

FIG. 1. (A) EM image of an AFM tip coated with poly-L-lysine (bar, 840 nm). (B) EM image of an AFM tip decorated with bacteria near the base of the tip. Bacteria generally attached on the sides of the pyramidal tip or more frequently near the base (bar, 640 nm).

filament's elastic properties. We show high-resolution images of *P. aeruginosa* PAO1 pili extending from cells dried onto the mica and have measured the interaction (or adhesion) forces of cells attached to AFM cantilever tips as the tips were brought down to the mica surface in water.

MATERIALS AND METHODS

Bacteria and growth conditions. *P. aeruginosa* PAO1, which expresses type IV pili under a variety of culture conditions, and PAK-Δpil, which carries a deletion of the pilin gene (for details, see reference 2), were used in this study. The cultures were maintained on Trypticase soy agar slants (Difco) until experimentation when they were grown on Trypticase soy broth (TSB) at 37°C. Bacteria were harvested at mid-exponential growth phase (optical density at 600 nm, 0.2) and washed three times in phosphate-buffered saline (PBS) (contained 5 mM KH_2PO_4, 25 mM Na_2HPO_4, and 120 mM NaCl, pH adjusted to 7.4 by using NaOH) by low-speed centrifugation, so as to avoid shear, and resuspended in PBS. The PAK-Δpil strain was used for the control experiment.

Sample preparation. In this study, mica, which has a very flat surface, was chosen as a support for the bacteria during both the structural and adhesion experiments. Immediately after the third wash of the bacteria in PBS, a drop of bacterial suspension was placed on a freshly cleaved mica surface. Excess fluid was drawn off and the bacteria allowed to adsorb for 15 min, after which the sample was rinsed with deionized water and air died at room temperature. Quick examination of all preparations by AFM was done so as to confirm the presence or absence of pili before more extensive studies were carried out.

Attachment of bacteria to AFM tips for force measurements. Sharpened silicon nitride AFM cantilevers were incubated overnight in a 0.1% (wt/vol) aqueous poly-L-lysine solution (Sigma Aldrich, St. Louis, MO). After this period, the cantilevers were removed and allowed to dry for 2 h by standing on edge on a paper towel. Then, a drop of bacteria suspension in PBS was placed at the tip of the poly-L-lysine-treated V-shaped AFM cantilever, and allowed to adsorb for 15 min. Cantilevers were then rinsed in PBS and used immediately, without drying, for force measurements. Scanning electron microscopy (SEM) was performed on all cantilevers coated with bacteria after AFM measurements to verify the presence of cells near the cantilever tip (Fig. 1). Unfortunately, SEM resolution was not sufficient to visualize the pili, but observation of similar cultures grown under similar conditions by using negative stains and transmission electron microscopy (TEM) revealed numerous pili (Fig. 2).

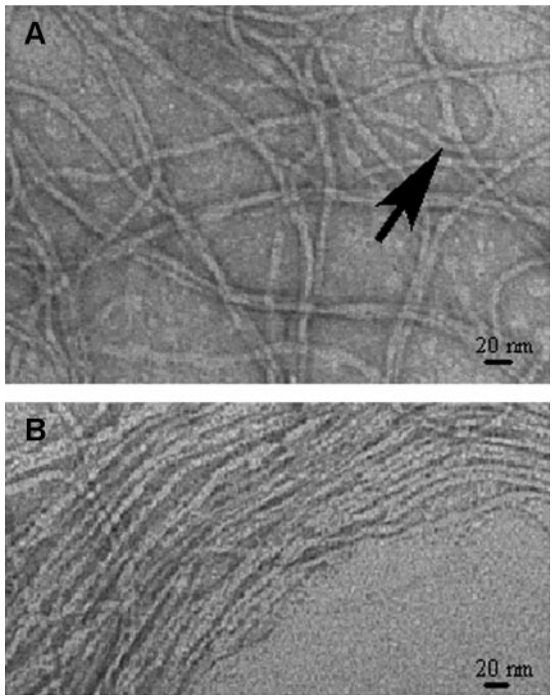

FIG. 2. TEM images of pili for *P. aeruginosa* PAO1. (A) Individual entangled pili. Sharp bends in the pili (arrow) were produced through the sample drying process. (B) Example of the tendency for pili to form bundles.

AFM imaging and force measurements. AFM images and force measurements were recorded using the contact mode at room temperature with a Molecular Imaging microscope. Images were recorded in both height and deflection modes. While height images provided quantitative information on sample surface topography, deflection images often exhibited higher contrast of morphological details. For imaging, V-shaped cantilevers with oxide-sharpened Si_3N_4 tips were used with spring constants of 8 ± 4 mN/m. Cantilever spring constants were determined by measuring the tip deflections for known applied forces as described by Jericho et al. (11). High-resolution images were recorded from dried preparations with optimized feedback parameters at scan frequencies of 4 Hz. Force measurements were performed between the bacteria on the AFM probe and a freshly cleaved mica surface in PBS solution. To engage pili with the mica surface, the tip was made to gently touch the surface with forces of less than 200 pN so as not to break or deform the pili. Control experiments consisted of using poly-L-lysine-coated AFM tips (no bacteria) or of replacing the *P. aeruginosa* PAO1 strain with PAK-Δpil mutants. The force measurements were then performed under the same conditions as discussed above. All retraction force curves were recorded at a cantilever retraction rate of 3 μm/s and an interaction time of 1 s.

Transmission electron microscopy. *P. aeruginosa* PAO1 was grown in TSB to an exponential growth phase (optical density at 600 nm, 0.2) at 37°C and the culture centrifuged at $8{,}000 \times g$ for 15 min to pellet cells for examination by TEM. Here, the cells were resuspended in deionized water and layered on a carbon- and Formvar-coated 200-mesh copper grid, which was then negatively stained with 2% (wt/vol) uranyl acetate for viewing. The cell-free culture supernatant was centrifuged at $20{,}000 \times g$ for 60 min and the pellet (consisting of pili, flagella, and other cellular debris) resuspended and stained as described for the cells (see above).

RESULTS

Transmission electron microscopy. When cultures of *P. aeruginosa* PAO1 were grown in TSB and negative stains made of the cells centrifuged from the broth, pili were frequently seen attached to the polar regions of the bacteria. These were of various lengths, since centrifugation introduced enough

shear into the culture to break the filaments from the cell. This was advantageous because the sheared pili could then be isolated from the supernatant by high-speed centrifugation for better dimensional analysis. The isolated pili were found as individual filaments, often entangled with one another (Fig. 2A) or as bundles of pili (Fig. 2B). In both cases, the diameter of the pili was 6 to 8 nm. Analysis of length could not be done, since the filaments had been sheared into various lengths. Interestingly, the forces that the filaments were subjected to during drying on the TEM grid were strong enough to bend them into various shapes (Fig. 2A).

Atomic force microscopy. Fig. 3 shows representative AFM images recorded in contact mode of the polar ends of intact cells of *P. aeruginosa* PAO1. The bacterial morphology, flagella, and pili were clearly visible at tip surface forces of about 1 to 1.5 nN. As seen in Fig. 3A, bacteria imaged in air have a flattened scalloped shape with raised edges due to dehydration effects and the convolution between the AFM tip and the cell surface. Figure 3A shows five polar pili and one flagellum extended individually and uniformly from the bacterial body and stretched over several micrometers. Figure 3B illustrates the difference between pili and flagella. It shows several pili and two 15- to 18-nm-diameter flagella as determined from AFM cross sections. Type IV pili frequently aggregate laterally to form bundles, as revealed by the high-resolution AFM image in Fig. 3B, and this confirms the TEM observation (Fig. 2B).

In all AFM images, the mica surfaces show dotlike features (Fig. 3A through C), embedded in a gel-like smooth surface layer. These dotlike features could have a variety of origins and could, for example, be due to aggregates coming from the outer membrane of the cells or they could be residual particulates from the culture medium. The occasional observation of "bare" mica patches was fortuitous, since pilus filaments could sometimes be seen to stretch across them. In all cases, a thin coating of adsorbed material was found to be covering these bare regions. In Fig. 3C, two pili cross such an empty area. This permitted measurement of the thickness of the coating, the pili, and the embedded depth of each pilus in the coating (Fig. 3D).

Figure 4 shows some pili fragments dispersed on the mica surface after an extensive wash of the surfaces shown in Fig. 3 with deionized distilled water. The rinsing step provided cleaner AFM images with fewer dotlike features. In Fig. 4, the overall architecture of the isolated pili is more clearly visible and an indication of their helical structure can be discerned (Fig. 4A, inset). As shown in Fig. 4A, the filaments are extremely long (up to 7 μm). Moreover, in accordance with the rodlike nature of the type IV pili, all the fragments are relatively straight and exhibited a smooth surface. The small diameters of these filaments can be easily measured by AFM cross sections. These diameters ranged from 4 to 6 nm for more than 20 pili measured in this study, while the thickness of the smooth layer was about 7 nm. The pilus diameter measured by AFM was reasonably close to that measured by TEM, especially when stain-filament interactions are taken into account (e.g., the pH of the uranyl acetate as a negative stain was approximately 4.2, which is unnaturally low; this could have resulted in charge-charge repulsion between pilin subunits to artificially expand the pilus diameter).

Force spectra. Fig. 5 displays several representative force retraction spectra. In these experiments, bacterium-coated

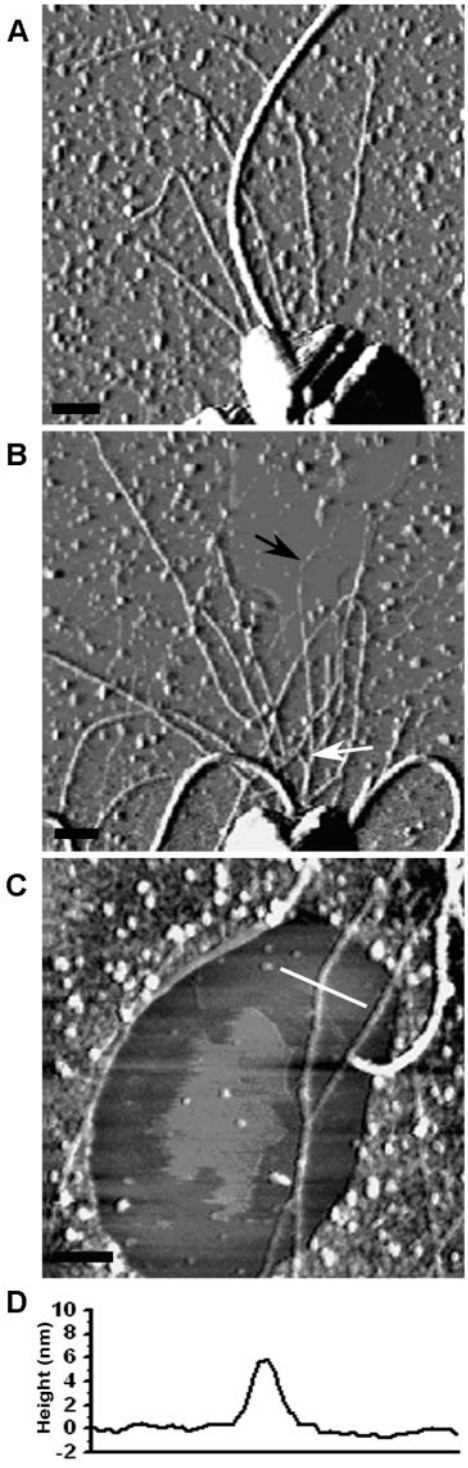

FIG. 3. (A) AFM image of the pole region of a *P. aeruginosa* PAO1 bacterium showing a flagellum and several straight pili. (B) Pili embedded in the layer of surface deposit. In some regions (black arrow), pili appear to be nearly submerged in a smooth region of the deposit. The white arrow points to a pili bundle. (C) Example of a bare region of the mica substrate traversed by pili fibers. (D) Cross section of the pilus in panel C along the line indicated. Such cross sections had pili diameters of 4 to 6 nm. Scale bars, 250 nm.

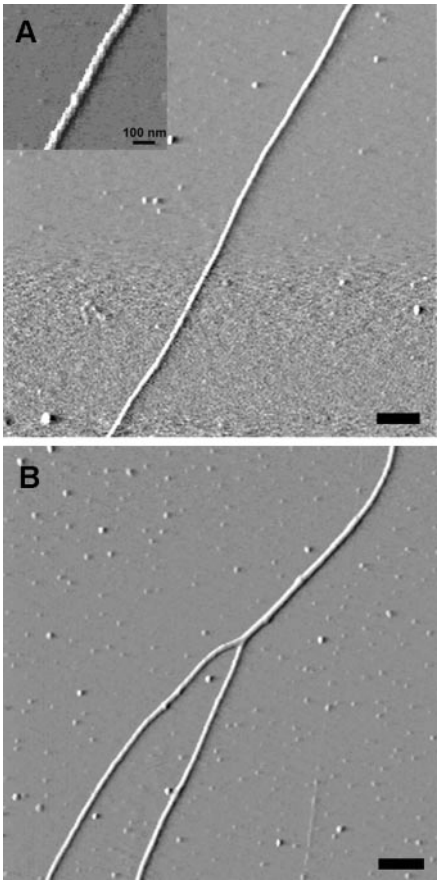

FIG. 4. (A) AFM image of a single straight pilus. The inset represents an enlarged region of the pilus and shows a helical fine structure on the pilus surface. (B) A frequently observed branching of pili. Scale bar, 300 nm.

AFM tips approached and retracted from mica surfaces under buffer. The spectra show the force pulling on the AFM tip (increased force is indicated by a downward direction) as a function of tip distance from the surface. A significant fraction (about 80%) of the retraction curves displayed single unbinding (or release) forces, while the remaining measurements showed multiple rupture events or no adhesion. Multiple force curves recorded at the same location of the mica surface yielded reproducible behavior. Figure 6A and B show the combined results of one hundred rupture events with the corresponding rupture lengths from a set of force retraction spectra taken using a single bacterium-coated AFM tip. The histogram of the rupture forces displayed a single maximum and a mean magnitude of 95 pN (Fig. 6A). More importantly, Fig. 5 and Fig. 6B reveal that most unbinding events were accompanied by nonlinear elongation forces and rupture lengths ranging from 0.4 to 3 μm. We suggest that these elongation forces and large rupture lengths are due to the pulling of extremely long pili. Similar data were obtained using five different probes and samples.

Force spectra for the control experiments were substantially different from those for *P. aeruginosa* PAO1 experiments and support our claim that the measured unbinding forces shown in Fig. 5 originate from pili that link bacteria attached to the

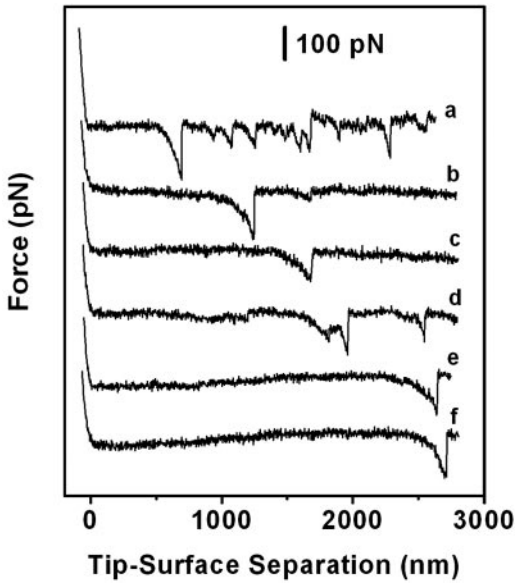

FIG. 5. (A) Collection of force spectra (retraction) taken with bacterium-coated tips over mica surfaces. Tip retraction speeds were 3 μm/s, and the spectra from a to f were arranged in order of increasing retraction distance needed to apply tension on the pili.

AFM cantilever with the mica surface. As shown in Fig. 6C (inset), for the bare poly-L-lysine-coated probes, the adhesion forces were much larger (~500 pN), while rupture lengths were in the 0- to 600-nm range (Fig. 6C). These observations indicate that the poly-L-lysine linker did not affect forces measured between the bacteria and the mica surface, and the results are in agreement with similar measurements by Lower et al. (16). A similar result was obtained for the PAK-Δpil mutant-coated probes. Here again adhesion forces were larger (~400 pN) (Fig. 6D, inset) and rupture lengths (10 to 100 nm) were very short. These data together led us to conclude that the measured forces in Fig. 5 reflect the interaction between the bacteria pili and the mica surface.

DISCUSSION

Imaging of pili. The imaging of pili via negative stains and TEM confirmed the general arrangement and bundling of the filaments that were initially seen by AFM using intact cells (compare Fig. 2 with Fig. 3A through C). The dimensional analysis of individual pili by the two microscopy techniques was also reasonably close when one considers compression forces due to drying (both TEM and AFM) and stain interactions with pilin subunits (TEM). AFM suggested the diameter of a pilus was in the order of 4 to 6 nm, whereas TEM suggested 6 to 8 nm. Both techniques suggested that on intact cells, the pili were located primarily at only one pole at a time and that their lengths varied from 0.5 to 7 μm. Surprisingly, TEM revealed good flexibility of the pili (Fig. 2A), which was indicative of weak pilin-pilin interaction. This observation was confirmed by the elastic response of the pili during the AFM adhesion force experiments.

AFM imaging in an aqueous environment of flexible structures, such as pili, is not possible at the present time, since the

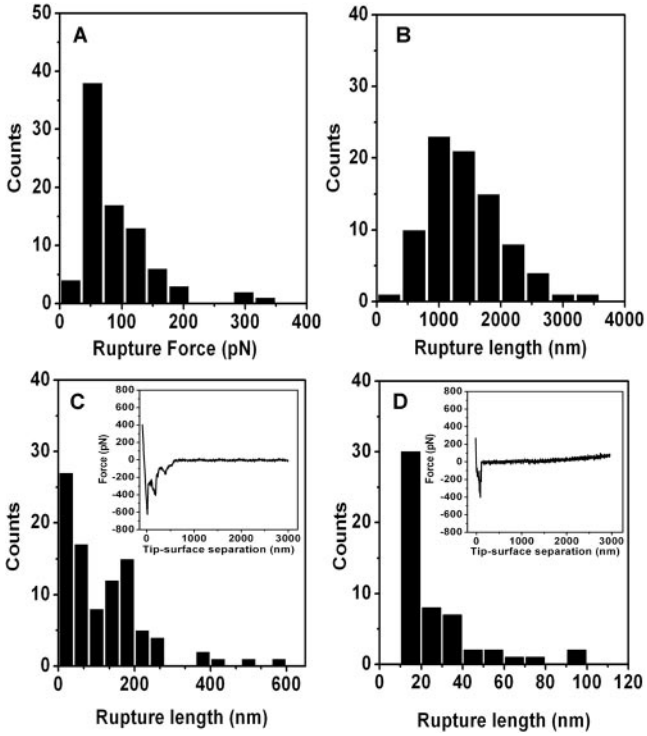

FIG. 6. (A) Distribution of observed rupture forces for pili force spectra over mica surfaces. A mean rupture force of 95 pN was obtained. (B) Distribution of corresponding piezo retraction distances needed for rupture. Corresponding pili lengths depend on the (unknown) positions of the bacteria on the AFM cantilever. (C) Distribution of piezo retraction distances for bond rupture for poly-L-lysine-coated AFM tip. No rupture lengths in excess of 600 nm were observed. The inset shows a typical force spectrum for poly-L-lysine. (D) Distribution of piezo retraction distances for bond rupture for strain PAK-Δpil without pili. No rupture lengths in excess of 100 nm were observed. The inset shows a typical force spectrum for strain PAK-Δpil.

tip forces required for imaging these filaments exceeds their adhesion forces; the tip easily dislodges them in a fluid medium. In this study, the pili were fortuitously stabilized against the imaging force exerted by the AFM tip when dried. During drying, a layer, presumably composed of bacteria derived material and culture residue (25), embedded the pili in a thin, smooth coating on the mica surface that did not inhibit imaging. In our air-dried samples, this layer allowed imaging, even against the inevitable capillary forces resulting from the inherent surface-water layer left on the specimen. As shown in Fig. 3, flagella and pili were easily distinguishable from one another by AFM, and the overall architecture and assembly pattern of the pili were clearly visible in these dry-state images. This surface eutectic is, however, unfavorable for the extreme high-resolution imaging, since the embedding of these narrow pili filaments tends to obscure the finer molecular detail. Repeated sample washing with water could detach pili from bacteria and repeated washing appeared to thin but never eliminate the surface layer. This thinning allowed finer detail, such as the helical pattern on the pili surface (Fig. 4A, inset), to be revealed.

Force spectra. Previous studies have demonstrated that bacterial pili are powerful retraction machines that can act as linear motors and that are responsible for the twitching motility observed in a variety of bacterial species (17, 18, 20, 29). Type IV pili also appear to be involved in a wide variety of other processes, such as biofilm formation, pilus-mediated bacteriophage infection, conjugation, and activation of certain host cell responses during pathogenesis. The dynamic aspects of pili extension and retraction were recently investigated with laser tweezers (17, 18, 20). In these studies, bacteria that were immobilized on latex beads with poly-L-lysine were tethered via a pilus to small beads in a laser trap. Measurements of the displacement of the small beads from the center of the trap allowed a determination of the forces exerted by pili during pili retraction. The retraction forces for *Neisseria gonorrhoeae*'s type IV pili were in excess of 100 pN (18). Although AFM force spectroscopy does not have the same sensitivity as optical tweezers, it is nevertheless of interest to compare the results of the two different techniques. To ensure a good comparison, we followed many of the same preparatory methods used in the optical tweezers experiment; we treated our AFM cantilevers and tips with poly-L-lysine to attach bacteria to the cantilever. Since, in the experiments with tweezers, the force-sensing beads became tethered to immobilized bacteria at distances of 1 to 3 μm, we lowered the AFM cantilever until the tip made contact with the substrate. Electron microscopy (EM) images showed that bacteria on the cantilevers were attached either to the sides of the pyramidal tips or more frequently near the base of the tips as shown in Fig. 1. Direct contact of bacteria with the substrate was thus avoided in most cases. Although flagella could also connect bacteria to the substrate, it is most likely that pili tethers were primarily involved, since they are a prime adhesin for *P. aeruginosa*.

The force spectra in Fig. 5 and the histogram in Fig. 6A show that at a tip retraction speed of 3 μm/s, bond rupture forces of 95 pN were developed in the type IV pili attached to the mica. Unlike Maier et al.'s experiment (17, 18), in which the pili themselves retracted and produced a pulling force, in our experiment, the AFM tip was retracted, pulling the attached pili until adherence was broken or the pilus filaments themselves broke. It is possible that our pili could also have actively contracted during our force experiments, but resulting corrections to the nonlinear portion of the force curve (near pulloff) would have amounted to not much more than 20 nm and would not be significant. Since active pili contraction was not observed, we assumed that pili were stationary during collection of the force spectra. Although multiple adhesion and release events were sometimes observed (first trace in Fig. 5), most force curves displayed single adhesion peaks. The similarity of the shape of these events for all the traces shown in Fig. 5 suggests that they most likely arose from forces acting on a single pilus. We thus interpret the initial flat regions in the force spectra in Fig. 5 as a "pilus-straightening" event (the entropic region) requiring minimal force. On further tip retraction, the tension on the pilus increases and the cantilever bends (thus exerting a force on the pilus) until the weakest part of the cell-pilus-mica system breaks. The cantilever then snaps back to its equilibrium position. On further tip retraction, this sequence of events is repeated for the next longest pilus link. This sequence of events is illustrated in Fig. 7A to C; it was assumed that the

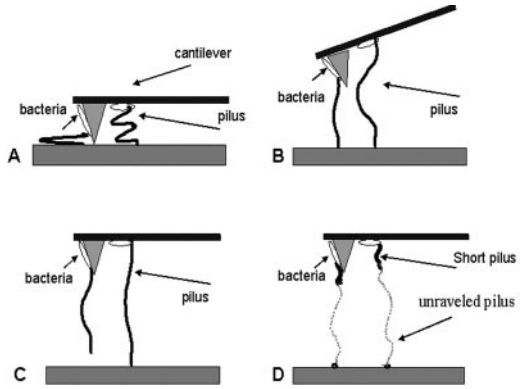

FIG. 7. Drawing showing possible ways in which pili can tether bacteria to a surface. In panel A, the tip touches the surface and long pili from bacteria near the tip apex or near the tip base are folded and adhere with their distal end to the mica surface. (B) On tip retraction, pili straighten out, and the shortest pili exerts a force on the cantilever, thus producing a force signature in the force spectrum. (C) On further retraction, some part of the bacterium-pili-substrate complex breaks (most likely the pili-substrate bond) and the cantilever returns to its neutral position. On further retraction, the above process will be repeated with the next longest pili. (D) An alternate model, discussed in the text, of the form of the tether that anchors bacteria to the substrate. Here, several turns of short pili fibers are unraveled and the constituent pilin molecules are denatured, thus forming a long amino acid chain with much lower persistence length than whole pili.

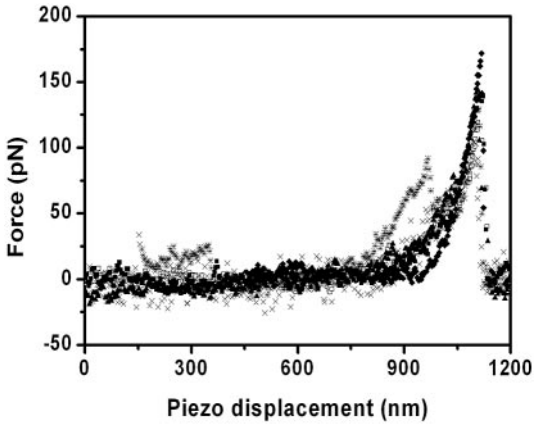

FIG. 8. Sections of force curves a, b, c, d, e, and f in Fig. 5 superimposed to illustrate the similarity of the slopes of the nearly linear regions near rupture. Individual traces were shifted horizontally until curves near the principal adhesion peaks overlapped at a force of 75 pN. The extra hump at 920 nm (derived from trace d in Fig. 5) is most likely caused by adhesion of two pili of nearly the same length.

break occurs at the pilus-mica bond. The magnitude of the adhesion force most likely depends on how the distal ends of pili interact with the mica surface. Since *P. aeruginosa* bacteria typically have a cluster of several pili at their poles (Fig. 3), the pili should be stretched and released from the mica surface sequentially as was possibly the case for the first trace in Fig. 5. The wide distribution of rupture length shown in Fig. 6B supports this multiple-fiber picture. The fact that a large number of force curves displayed a single adhesion peak, however, suggests that we are dealing with individual fibers in most cases.

Interpretation of the force spectra. The main features of the force curves are long regions of near-zero force, followed by a gradual rise in the force to a nearly linear region that is terminated by an abrupt release of the cantilever. Normalization of force curves by division of each curve by the corresponding contour length was not possible, since the position of bacteria on the cantilevers and hence the pili contour length could not be determined. The similarity of all force curves shown in Fig. 5 was therefore brought out by shifting the curves along the horizontal axis and superimposing them at a particular force value. Figure 8 shows such a superposition at a force of 75 pN. All curves show an initial nonlinear increase in force followed by a region where the force increases in a nearly linear fashion with pili extension. We performed regression analysis for these slopes, and the resulting values are summarized in Table 1. We attribute the low value for trace c to the somewhat lower rupture force for this trace, which meant that the linear region was not reached. It is interesting that these values are similar to the value determined by Maier et al. (17) from force-distance curves for type IV pili from *pilT* mutant cells of *Neisseria gonorrhoeae*. This provides further support for our assertion that the force curves in Fig. 5 represent the stretching of pili.

The detailed interpretation of the force curves is more problematic. The observation that all force curves have very similar shapes, irrespective of the pilus length, shows that the slopes for the nearly linear region (Table 1) cannot represent a simple springlike modulus of a pilus. Depending on where a bacterium was attached on the AFM tip, the ratio of the length of the longest pilus (curve f) to the shortest (curve a) in Fig. 5 ranged from a factor of 2 (all bacteria assumed attached near the base of the tip) to 5 (all bacteria assumed attached close to the tip apex). SEM images taken of several bacterium-coated tips showed that bacteria attached on the tip sides near the apex or near the tip base. Since the spring constant of a Hooklike spring is inversely proportional to the length of the spring, the slope of the nearly linear region close to the breakpoints should have varied by no less than a factor of 2 going from trace a to trace f in Fig. 5. The absence of a significant pilus-length dependence of the force curves thus suggests to us that the nearly linear region in the force curves cannot be directly related to a pilus elastic modulus.

The origins of the nonlinear parts of the force-distance curves in Fig. 5 are not clear. Such nonlinear effects are generally attributed to entropic effects. Force spectra of biological polymers are frequently discussed in terms of the wormlike-chain (WLC) model (22) or the freely jointed-chain (FJC) model (24), where entropy provides the elastic restoring force when an uncoiled polymer is subjected to an end-to-end

TABLE 1. Slopes near rupture for the force curves in Fig. 5

Trace	Slope (pN/nm) ± SE
a	1.3 ± 0.06
b	1.3 ± 0.1
c	0.7 ± 0.1
d	1.5 ± 0.1
e	1.0 ± 0.15
f	1.15 ± 0.1

stretching force. The WLC model was also successfully applied recently in the analysis of AFM experiments on the unfolding of transmembrane proteins on live bacteria (15). The FJC model pictures the polymer as a chain of rigid segments that are free to rotate at the segment joints. The WLC model, on the other hand, views the polymer as a continuous flexible rope. The model is characterized by only two parameters, the polymer persistence length, p, and the polymer contour length, L, at zero applied force. The persistence length is the distance over which a polymer shows significant bending under thermal fluctuations. A polymer will appear relatively straight if the persistence length is large compared to the contour length. Stretching curves for polypeptides have been fitted successfully with persistence lengths around 0.5 nm. The persistence length of type IV pili on the other hand has been reported to be 5 μm (29). Such a large persistence length implies that type IV pili are much stiffer than unfolded proteins, and a slow increase in force with extension as observed in our data is not expected. A fit of the basic WLC model to the force curves with a p of 5 μm was therefore impossible. The WLC model for a p between 0.4 to 0.8 nm also did not produce a convincing fit for the curves in Fig. 5. Fitting attempts with the FJC model were also not successful. The FJC model is often extended to allow for segment elasticity that arises from bond angle torsion and bending (23). This extensible FJC model was also tried but, as expected, gave a slope near rupture that depended on the polymer length.

Reasonable fits to all curves, however, could be obtained if we included a single elastic spring of spring constant, k_s, in series with the structure. The equation for the force in this case is given by the following equation:

$$F = (k_bT/p) \times \{0.25 \times [1 - (Z - F/k_s)/L] - 2 + (Z - F/k_s)/L) - 0.25\}$$

where Z is the end-to-end distance of the polymer, T is the absolute temperature and k_b is Boltsmann's constant. In the evaluation of this equation, Z was determined from a specified force by solver routines. For the experimental curves, the distance Z was the piezo retraction distance, with the origin determined from the intersections of the extrapolations of the hard-surface slopes (far left region for the force curves in Fig. 5) with the horizontal axis. An example of such a fit is shown in Fig. 9. The figure shows the experimental data for the first (and largest) force signature in trace a in Fig. 5 as well as the WLC result for a p of 0.8 nm, an L of 600 nm, and a k_s of 0.002 N/m. Also shown is the basic WLC result with the spring omitted. Similar fits with the same values for p and k_s, but with pilus lengths as an adjustable parameter, were obtained for the other traces in Fig. 5. The WLC model thus described the shape of the force curves in Fig. 5 reasonably well, but a linear term was needed to obtain a good fit.

An explanation for the initial curvature in the force curves with the previous equation required a persistence length that seems unrealistic for a type IV pilus. The latter value is more appropriate for unfolded protein polymers where p is of the size of an amino acid. With a persistence length in the range of micrometers, a pilus will have a high bending modulus and the force curves are not expected to show the gradual increase in force with extension that reflect entopic contributions to the elastic response. The significance of the fit with the WLC model is thus not clear.

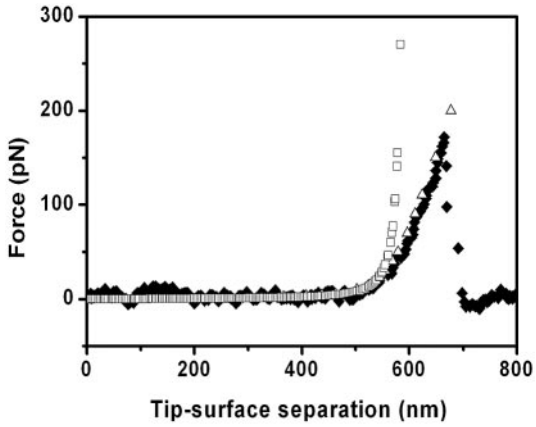

FIG. 9. ◆, cantilever force as function of tip-surface separation distance for the first adhesion feature in trace a in Fig. 5. The zero for the horizontal axis was taken as the first position in the traces in Fig. 5 where the cantilever deflection on retraction was zero. □, WLC model with persistence length of 0.8 nm and contour length of 600 nm. For larger values for L, the curvature of the force curve as it approaches the nearly linear region could not be reproduced for reasonable persistence lengths. Δ, WLC model with a p of 0.8 nm, a L of 600 nm, and a linear spring with spring constant of 0.002 N/m. With the same linear spring included, the WLC model could be fitted to the main features in the other force curves shown in Fig. 5.

Elastic properties of the end subunit of a pilus. The distal end of a pilus plays a major role in the attachment of the pili to a surface. Type IV pili are required for the attachment of a number of pathogens to human epithelial cells in the early stages of infection (8). The attachment to receptors can also involve a complex association of a number of other pilus adhesins (such as PilC) with molecular masses of ~110 kDa (3). The basis of the nonspecific adhesion we see here with our experimentation of pili to a mica surface, and hence the interpretation of the observed rupture forces, is not clear. The low persistence length needed to interpret the force curves in terms of an entopic force contribution might suggest that the pili helix and the corresponding pilin molecules are partially unraveled as depicted in Fig. 7D. For example, for a 149-amino-acid-sized mature pilin molecule, its end-to-end contour length at zero force would be about 75 nm so that about eight pilin molecules (equivalent to 1.5 turns of the helix) would have to be uncoiled to explain the force curve in Fig. 9. Correspondingly larger numbers of turns of the helix would have to be unraveled for the other force curves in Fig. 5. Although uncoiling of the pilin structure has been observed for type P pili (10), this is not thought to happen with type IV pili. It therefore seems unlikely that the pilus-mica bond region is responsible for the observed force spectra.

Elastic properties of the cell wall to which a pilus is attached. The small variations of the spring constants in Table 1 show that the same spring must be present for all the different-length pili in Fig. 5. This suggests that the common source of this spring might be the attachment region of the pilus to the bacterial wall. The current picture of pili attachment has the pilus filament pass through a PilQ collar that is embedded in the outer membrane of the cell wall (12). Pilus assembly and

disassembly (retraction) take place at the inner (plasma) membrane with the help of a large range of Pil proteins (12). At a rupture force of 100 pN, the linear spring with a spring constant of 0.002 N/m (WLC model fit) would extend a distance of about 50 nm. The cell wall would thus have to stretch by a comparable amount. The outer membrane is known to be naturally deformable because formation of membrane vesicles with diameters of 50 to 100 nm is frequently observed in gram-negative bacteria (30). Membrane deformation, when tensile forces of 100 pN or more are applied to pili, may thus play a role for pili that are anchored to the outer membrane, such as P pili for *E. coli* bacteria, and pili extension experiments may thus also give information on the elastic properties of the bacterial wall. For type IV pili in *P. aeruginosa*, however, in which the pili are anchored to the plasma membrane, the peptidoglycan layer (35) will be stretched taut by the turgor pressure within the cell and will not accommodate much more extension. The source of the linear spring component suggested by our experiments is thus difficult to place at present.

In summary, we showed that AFM can give high-resolution images of type IV pili and that AFM force sensitivity is sufficient to probe their elastic properties. The observed force extension curves for pili from *Pseudomonas aeruginosa* were qualitatively similar to the nonlinear stretching curves that have been reported for a large variety of biopolymers. The force spectra could be fitted with the WLC model if a term representing a linear elastic spring was included. The persistence length required for a fit was, however, not in agreement with reported persistence length for type IV pili. The observation that the spring constant for the linear spring was independent of the pili length suggests that it does not represent the elastic properties of a whole pilus but of a fixed elastic element somewhere in the mica-pilus-bacterium system.

ACKNOWLEDGMENTS

Most experimentation was performed in the laboratory of M.H.J., which is funded by an NSERC-Discovery grant to M.H.J. J.M.B. is supported by the National Research Council of Canada's Genomics and Health Initiative (2005-42561). We are indebted to Sarah Schooling of the laboratory of T.J.B. for the electron micrographs of PAO1 pili that were taken in the Guelph Regional Integrated Imaging Facility, which is partially funded through an NSERC-Major Facilities Access grant to T.J.B. Research performed in the laboratory of T.J.B. was funded by an NSERC-Discovery grant as well as by funds through the AFM net-NCE to T.J.B.

REFERENCES

1. **Bieber, D., S. W. Ramer, C. Y. Wu, W. J. Murray, T. Tobe, R. Fernandez, and G. K. Schoolnik.** 1998. Type IV pili, transient bacterial aggregates, and virulence of enteropathogenic *Escherichia coli*. Science **280:**2114–2118.
2. **Boyd, J., T. Koga, and S. Lory.** 1994. Identification and characterization of PilS, an essential regulator of pilin expression in pseudomonas aeruginosa. Mol. Gen. Genet. **243:**565–574.
3. **Craig, L., M. E. Pique, and J. A. Tainer.** 2004. Type IV pilus structure and bacterial pathogenicity. Nat. Rev. Microbiol. **2:**363–378.
4. **Craig, L., R. K. Taylor, M. E. Pique, B. D. Adair, A. S. Arvai, M. Singh, S. J. Lloyed, D. S. Shin, E. D. Getzoff, M. Yeager, K. T. Forest, and J. A. Tainer.** 2003. Type IV pilin structure and assembly: X-ray and EM analyses of *Vibrio cholaere* toxin-coregulated pilus and *Pseudomonas aeruginosa* PAK pilin. Mol. Cell **11:**1139–1150.
5. **Dufrêne, Y. F.** 2004. Using nanotechniques to explore microbial surfaces. Nat. Rev. Microbiol. **2:**451–460.
6. **Durand, E., A. Bernadac, G. Ball, A. Lazdunski, J. N. Sturgis, and A. Filloux.** 2003. Type II protein secretion in *Pseudomonas aeruginosa*: the pseudopilus is a multifibrillar and adhesive structure. J. Bacteriol. **185:**2749–2758.
7. **Emerson, R. J., and T. A. Camesano.** 2004. Nanoscale investigation of pathogenic microbial adhesion to a biomaterial. Appl. Environ. Microbiol. **70:**6012–6022.
8. **Hanne, C. W.-L., F. T. Hegge, M. Wolfgang, S. F. Hayes, J. P. M. van Putten, and M. Koomey.** 2001. *Neisseria gonorrhoeae* PilV, a type IV pilus-associated protein essential to human epithelial cell adherence. Proc. Natl. Acad. Sci. USA **98:**15276–15281.
9. **Harshey, R. M.** 2003. Bacterial motility on a surface: many ways to a common goal. Annu. Rev. Microbiol. **57:**249–273.
10. **Jass, J., S. Schedin, E. Fällman, J. Ohlsson, U. Nilsson, B. E. Uhlin, and O. Axner.** 2004. Physical properties of *Escherichia coli* P pili measured by optical tweezers. Biophys. J. **87:**4271–4283.
11. **Jericho, S. K., and M. H. Jericho.** 2002. Device for the determination of spring constants of atomic force microscope cantilevers and micromachined springs. Rev. Sci. Instrum. **73:**2483–2485.
12. **Keizer, D. W., C. M. Slupsky, M. Kalisiak, A. P. Campbell, M. P. Crumpi, P. A. Sastry, B. Hazes, R. T. Irvin, and B. D. Sykes.** 2001. Structure of a pilin monomer from *Pseudomonas aeruginosa*. J. Biol. Chem. **276:**24186–24193.
13. **Klausen, M., A. Heydorn, P. Ragas, L. Lambertsen, A. Aaes-Jørgensen, S. Molin, and T. Tolker-Nielsen.** 2003. Biofilm formation by *Pseudomonas aeruginosa* wild type, flagella and type IV pili mutants. Mol. Microbiol. **48:**1511–1524.
14. **Liang, M. N., S. P. Smith, S. J. Metallo, I. S. Choi, M. Prentiss, and G. M. Whitesides.** 2000. Measuring the forces involved in polyvalent adhesion of uropathogenic *Escherichia coli* to mannose-presenting surfaces. Proc. Natl. Acad. Sci. USA **97:**13092–13096.
15. **Lower, B. H., R. Yongsunthon, F. P. Vellano III, and S. K. Lower.** 2005. Simultaneous force and fluorescence measurements of a protein that forms a bond between a living bacterium and a solid surface. J. Bacteriol. **187:**2127–2137.
16. **Lower, S. K., C. J. Tadanier, and M. F. Hochella.** 2000. Measuring interfacial and adhesion forces between bacteria and mineral surfaces with biological force microscopy. Geochim. Cosmochim. Acta **64:**3133–3139.
17. **Maier, B., M. Koomey, and M. P. Sheetz.** 2004. A force-dependent switch reverses type IV pilus retraction. Proc. Natl. Acad. Sci. USA **101:**10961–10966.
18. **Maier, B., L. Potter, M. So, H. S. Seifert, and M. P. Sheetz.** 2002. Single pilus motor forces exceed 100 pN. Proc. Natl. Acad. Sci. USA **99:**16012–16017.
19. **McBride, M. J.** 2001. Bacterial gliding motility: multiple mechanisms for cell movement over surfaces. Annu. Rev. Microbiol. **55:**49–75.
20. **Merz, A. J., M. So, and M. P. Sheetz.** 2000. Pilus retraction powers bacterial twitching motility. Nature **407:**98–102.
21. **Mu, X. Q., E. H. Egelman, and E. Bullitt.** 2002. Structure and function of hib pili from *Haemophilus influenzae* type b. J. Bacteriol. **184:**4868–4874.
22. **Odijik, T.** 1995. Stiff chains and filaments under tension. Macromolecules **28:**7016–7018.
23. **Oesterhelt, F., M. Rief, and H. E. Gaub.** 1999. Single molecule force spectroscopy by AFM indicates helical structure of poly(ethylene-glycol) in water. New J. Phys. **1:**6.1–6.11.
24. **Ortiz, C., and C. Hadziioannou.** 1999. Entropic elasticity of single polymer chains of poly(methacrylic acid) measured by atomic force microscopy. Macromolecules **32:**780–787.
25. **Pelling, A. E., L. Yinuo, S. Wenyuan, and J. K. Gimzewski.** 2005. Nanoscale visualization and characterization of *Myxococcus Xanthus* cells with atomic force microscopy. Proc. Natl. Acad. Sci. USA **102:**6484–6489.
26. **Razatos, A., Y.-L. Ong, F. Boulay, D. L. Elbert, J. A. Hubbell, M. M. Sharma, and G. Georgiou.** 2000. Force measurements between bacteria and poly(ethylene glycol)-coated surfaces. Langmuir **16:**9155–9158.
27. **Sauer, F. G., M. Barnhart, D. Choudhury, S. D. Knight, G. Waksman, and S. J. Hultgren.** 2000. Chaperone-assisted pilus assembly and bacterial attachment. Curr. Opin. Struct. Biol. **10:**548–556.
28. **Sauvonnet, N., P. Gounon, and A. P. Pugsley.** 2000. PpdD Type IV pilin of *Escherichia coli* K-12 can be assembled into pili in *Pseudomonas aeruginosa*. J. Bacteriol. **182:**848–854.
29. **Skerker, J. M., and H. C. Berg.** 2001. Direct observation of extension and retraction of type IV pili. Proc. Natl. Acad. Sci. USA **98:**6901–6904.
30. **Stoica, O., A. Tuanyok, X. W. Yao, M. H. Jericho, D. Pink, and T. J. Beveridge.** 2003. Elasticity of membrane vesicles isolated from *Pseudomonas aeruginosa*. Langmuir **19:**10916–10924.
31. **Sun, H., D. R. Zusman, and W. Shi.** 2000. Type IV pilus of *Myxococcus xanthus* is a motility apparatus controlled by the *frz* chemosensory system. Curr. Biol. **10:**1143–1146.
32. **Touhami, A., M. H. Jericho, and T. J. Beveridge.** 2004. Atomic force microscopy of cell growth and division in *staphylococcus aureus*. J. Bacteriol. **186:**3286–3295.
33. **Vallet, I., J. W. Olson, S. Lory, A. Lazdunski, and A. Filloux.** 2001. The chaperone/usher pathways of *Pseudomonas aeruginosa*: identification of fimbrial gene clusters (cup) and their involvement in biofilm formation. Proc. Natl. Acad. Sci. USA **98:**6911–6916.
34. **Wall, D., and D. Kaiser.** 1999. Type IV pili and cell motility. Mol. Microbiol. **32:**1–10.
35. **Yao, X., J. Walter, S. Burke, S. Stewart, M. H. Jericho, D. Pink, R. Hunter, and T. J. Beveridge.** 2002. Atomic force microscopy and theoretical considerations of surface properties and turgor pressures of bacteria. Colloids Surf. B **23:**213–230.